Mechanism of contact angle saturation and an energy-based model for electrowetting*

Rui Zhao(赵瑞) and Zhong-Cheng Liang(梁忠诚)†

College of Optoelectronic Engineering, Center of Optofluidic Technology, Nanjing University of Posts and Telecommunications, Nanjing 210023, *China*

(Received 28 October 2015; revised manuscript received 18 January 2016; published online 20 April 2016)

Electrowetting, as a well-known approach to increasing droplet wettability on a solid surface by electrical bias, has broad applications. However, it is limited by contact angle saturation at large voltage. Although several debated hypotheses have been proposed to describe it, the physical origin of contact angle saturation still remains obscure. In this work, the physical factors responsible for the onset of contact angle saturation are explored, and the correlated theoretical models are established to characterize electrowetting behavior. Combination of the proper 3-phase system employed succeeds in dropping the saturating contact angle below 25°, and validates that the contact angle saturation is not a result of device-related imperfection.

Keywords: electrowetting, contact angle, saturation

PACS: 68.08.Bc, 68.08.–p, 68.03.Cd **DOI:** 10.1088/1674-1056/25/6/066801

1. Introduction

Electrowetting refers to reducing the contact angle of droplets by applying a voltage between a droplet and a dielectric coated electrode, which has found numerous potential applications in lab-on-chip,[1,2] optics,[3,4] and displays.[5–7] The contact angle change with voltage, described by the Young–Lippmann equation, predicts that the contact angle can be modulated to zero by increasing the voltage. However, the contact angle in fact reduces to a non-zero contact angle value beyond a critical external voltage, which deviates from the basic electrowetting theory, i.e., the Young–Lippmann equation. This phenomenon is widely known as contact angle saturation,[8–12] which restricts the electrowetting-based applications.[12–14]

In recent years, more and more investigations focused on exploring the underlying mechanisms responsible for contact angle saturation.[12–16] Several debated hypotheses such as dielectric breakdown,[11] zero interfacial tension,[12] charge trapping,[13] and air ionization[14] have been proposed to ascertain this saturation phenomenon. Unfortunately, the physical origin of contact angle saturation is still poorly clarified, and the relevant theory that can directly predict the onset of the saturation and reducing the saturation of contact angle for a specific system, is scarce.

In this work, the physical origins of contact angle saturation are explored, and also a theoretical model is constructed to describe the variation of contact angle change with applied voltage at higher voltage. In the experiment, a 3-phase system consisting of different combinations of conductive fluid and oil is employed to measure the saturating contact angle response to the increasing voltage. We deduce that electrowetting saturation is dominated by the interfacial tension of the 3-phase system and the surface tension of conductive liquid. The saturating contact angle occurs once ions escape from the main droplet and form into small droplets. The relevant results will enrich the theory of electrowetting saturation and expand its application scope in electrowetting devices where an even larger range of contact angle modulation is desired.

2. Theoretical calculation of contact angle saturation

Here we divide the electrowetting evolution into three stages: the first stage is that the change of cosine of the apparent contact angle (θ_v) with voltage can be well described by the Young–Lippmann equation,[2] the second stage starts when the cosine of the contact angle deviates from the parabolic behavior predicted by the Young–Lippmann equation and ends when the contact angle ceases to respond to voltage, and the onset of the third stage corresponds to the point where the contact angle stops decreasing and keeps constant.

The classification criterion of the electrowetting evolution mentioned above mainly rests on the force analysis around the triple contact line and interface. When the applied voltage is low, the triple contact line is pinned and the local contact angle remains equal to Young angle θ_Y.[16–18] The increase in electrostatic force tends to reduce the apparent angle θ_v while the local angle θ_Y keeps constant.[18] The transition from the first stage to the second stage depends on the movement of

*Project supported by the Fund from the Research Center of Optical Communications Engineering & Technology, Jiangsu Province, China (Grant No. ZSF0402).

†Corresponding author. E-mail: zcliang@njupt.edu.cn

© 2016 Chinese Physical Society and IOP Publishing Ltd

the triple contact line, herein the potential point is defined as the first threshold potential ($V_{\rm Th1}$). Beyond $V_{\rm th1}$, the electrowetting force is strong enough to conquer the pinning force at triple phase contact line and drive the triple contact line into movement, accordingly the electrowetting evolves into the second-stage. In this stage, the oil viscous effect, oil resistance, and dynamic friction hinder the movement of triple contact line and result in the discrepancy between the electrowetting behavior and the Young–Lippmann equation.[17] Keeping on increasing the voltage, the growing electrostatic force will eventually exceed the bonding force acting on the ions (or charges). The ions (or charges) start to escape from the main droplet once the interfacial tension can neither hold the ion(or charges) nor balance the electrowetting force,[19] here the point of potential is called the second threshold voltage $V_{\rm Th2}$. When $V > V_{\rm Th2}$, the contact angle stops decreasing and the corresponding electrowetting evolution transfers from the second stage to the third stage.

According to the classification listed above, the Young–Lippmann equation is accurate to describe the first stage, and the contact angle keeps constant in the third stage. The following work mainly focuses on the second stage. A theoretical model is established to predict the variation of transient contact angle with higher potential for the second stage. Since the size of droplet is smaller than the capillary length (droplet volume is 0.5 μl), the surface tension has an influence on the droplet shape while the gravity is ignored.[20] To simplify the problem, the droplet is considered to remain spherical in shape in the electrowetting process, which is illustrated in Fig. 1. Assume that the volume, side surface area, base surface, radius and height of droplet, and contact angle are V_0, $A_{\rm s}$, $A_{\rm b}$, R, $R+h$, and θ, respectively, where $h=-R\cos\theta$, according to the calculation formulas of the volume and area for the spherical segment, then we will have the following relationships:

$$V_0=\frac{1}{3}\pi R^3\left(2-3\cos\theta+\cos^3\theta\right), \tag{1}$$

$$A_{\rm s}=2\pi R^2\left(1-\cos\theta\right), \tag{2}$$

$$A_{\rm b}=\pi R^2\sin^2\theta. \tag{3}$$

Differentiating Eqs. (1)–(3), we can achieve the following equations:

$$\begin{aligned}{\rm d}V_0 &= \frac{\partial V_0}{\partial R}{\rm d}R+\frac{\partial V_0}{\partial\theta}{\rm d}\theta\\ &= \pi R^2\left(2-3cos\theta+\cos^3\theta\right){\rm d}R\\ &\quad+\frac{1}{3}\pi R^3\left(3\sin\theta-3\cos^2\theta\sin\theta\right){\rm d}\theta,\end{aligned} \tag{4}$$

$${\rm d}A_{\rm s} = 4\pi R\left(1-\cos\theta\right){\rm d}R+2\pi R^2\sin\theta\,{\rm d}\theta, \tag{5}$$

$${\rm d}A_{\rm b} = 2\pi R\sin^2\theta\,{\rm d}R+2\pi R^2\sin\theta\cos\theta\,{\rm d}\theta. \tag{6}$$

Assuming that the droplet volume keeps constant, the differential equation of droplet volume equals zero, i.e., ${\rm d}V_0=0$, and consequently

$$\frac{{\rm d}R}{{\rm d}\theta}=-R\sin^3\theta/(2-3\cos\theta+\cos^3\theta). \tag{7}$$

The changes of Helmholtz free energy from the side and base tension energy because of the droplet spreading, are

$${\rm d}F_{\rm s} = \gamma_{\rm ci}\,{\rm d}A_{\rm s}=\gamma_{\rm ci}\left(2\pi R\sin^2\theta\,{\rm d}R+2\pi R^2\sin\theta\cos\theta\,{\rm d}\theta\right), \tag{8}$$

$$\begin{aligned}{\rm d}F_{\rm b} &= \left(\gamma_{\rm cd}-\gamma_{\rm id}\right){\rm d}A_{\rm b}\\ &= \left(\gamma_{\rm cd}-\gamma_{\rm id}\right)\left(2\pi R\sin^2\theta\,{\rm d}R+2\pi R^2\sin\theta\cos\theta\,{\rm d}\theta\right)\\ &= -\gamma_{\rm ci}\cos\theta_Y\left(2\pi R\sin^2\theta\,{\rm d}R+2\pi R^2\sin\theta\cos\theta\,{\rm d}\theta\right).\end{aligned} \tag{9}$$

Here $\gamma_{\rm ci}$, $\gamma_{\rm cd}$, and $\gamma_{\rm id}$ denote the interfacial tension between conductive fluid and insulating fluid, conductive fluid and dielectric surface, and insulating fluid and dielectric surface, respectively.

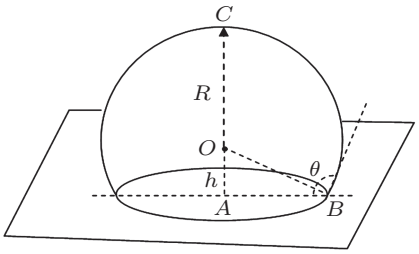


Fig. 1. Diagram of a droplet with radius R and contact angle θ.

When the potential V is applied to the electrowetting system, change of Helmholtz free energy induced by electrostatic energy is

$${\rm d}F_{\rm e}=-\frac{\varepsilon_0\varepsilon_{\rm r}}{2d}V^2{\rm d}A_{\rm b}, \tag{10}$$

where $\varepsilon_{\rm r}$ and ε_0 are the relative permittivity of the dielectric layer and the dielectric constant in a vacuum, d is the thickness of the dielectric layer.

Substituting Eq. (6) into Eq. (10), we can obtain

$${\rm d}F_{\rm e}=-\frac{\pi\varepsilon_0\varepsilon_{\rm r}}{\rm d}RV^2\left(\sin^2\theta\,{\rm d}R+R\sin\theta\cos\theta\,{\rm d}\theta\right). \tag{11}$$

During the droplet spreading and contact line movement, the energy dissipation is dominated by the viscous effect, drag force, oil resistance, and dynamic friction around the triple contact line.[21]

The viscous friction force and drag force of the moving contact line are linear with respect to the velocity of droplet edge movement[17,21]

$$F_{\rm v}=k_{\rm v}U, \tag{12}$$

where $k_{\rm v}=(k_1\mu+\xi)$, k_1 is a constant, μ is the viscosity of insulating fluid, and U is the velocity of contact line. The dynamic contact line friction force due to the three phase contact line movement is expressed as

$$F_{\rm f}=k_{\rm f}U^{0.3}, \tag{13}$$

where $k_f = k_2\gamma_{ci}$, k_2 is a constant. The velocity of contact line U is expressed as[22,23]

$$U = \frac{\gamma_{ci}}{\mu}\frac{\theta}{6n}\left(\frac{\varepsilon_0\varepsilon_r}{2d\gamma_{ci}}V^2 - \frac{\alpha}{\gamma_{ci}}\right). \tag{14}$$

Here, $n \sim 10$ is the logarithm of macroscopic length over microscopic length, and α is a constant. For simplicity, equation (14) is rewritten as

$$U = k_0 V^2, \tag{14a}$$

where $k_0 = \varepsilon_0\varepsilon_r\theta/12\mu n d\gamma_{ci}$.

The components of energy dissipation caused by the viscous effect, oil resistance and dynamic friction are shown as[22]

$$\begin{aligned} dF_{ds} &= (F_v + F_f)\, dA_s \\ &= \left[k_v U + k_f U^{0.3}\right](4\pi R(1-\cos\theta)\, dR \\ &\quad + 2\pi R^2 \sin\theta\, d\theta). \end{aligned} \tag{15}$$

The total change of Helmholtz free energy is expressed as

$$dF = dF_s + dF_b + dF_e + dF_{ds}. \tag{16}$$

The electrowetting system satisfies the Helmholtz free energy minimization once it reaches equilibrium, one can have

$$dF = dF_s + dF_b + dF_d + dF_e = 0. \tag{17}$$

Substituting Eqs. (7), (8), (9), (11), (14a), and (15) into Eq. (17) yields

$$\cos\theta = \frac{\cos\theta_1 + \dfrac{\varepsilon_0\varepsilon_r}{2d\gamma_{ci}}V^2}{1+\alpha_1 V^2 + \alpha_2 V^{0.6}}, \tag{18}$$

where θ_1 is the value of contact angle at potential V_{Th1}, $\alpha_1 = k_0 k_v/\gamma_{ci}$, $\alpha_2 = k_0 k_f/\gamma_{ci}$, and $V_{Th1} < V \le V_{Th2}$.

The relation for the whole electrowetting evolution is shown below

$$\cos\theta_v = \begin{cases} \cos\theta_Y + \dfrac{\varepsilon_0\varepsilon_r}{2d\gamma_{ci}}V^2, & V \le V_{Th1}, \\ \dfrac{\cos\theta_1 + \dfrac{\varepsilon_0\varepsilon_r}{2d\gamma_{ci}}V^2}{1+\alpha_1 V^2 + \alpha_2 V^{0.6}}, & V_{Th1} < V \le V_{Th2}, \\ \cos\theta_2, & V > V_{Th2}, \end{cases} \tag{19}$$

where θ_Y is the initial contact angle, θ_1 and θ_2 are the contact angles detected at the point of potentials V_{Th1} and V_{Th2} respectively, $\alpha_1 = k_0 k_v/\gamma_{ci}$ and $\alpha_2 = k_0 k_f/\gamma_{ci}$ are determined by fitting the equation to the experimental data at the point of the first threshold potential. If accurate parameters are required, it can be calculated by employing the exact expression for the velocity of the triple contact line given in Eq. (14).

The threshold voltages V_{Th1} and V_{Th2} in Eq. (19) can be theoretically derived based on our theories listed above. When $V = V_{Th1}$, the electrowetting force F_{el} is larger than the sum of the maximum static friction force F_p and capillary force F_{cap}, and then triggers the triple contact line moving.[16] Consequently

$$F_{el} \ge F_{cap} + F_p, \tag{20}$$

where $F_{el} = 2\eta\gamma_{ci}$ is the electrowetting force acting on the contact line, the capillary force is $F_{cap} = \gamma_{ci}(\cos\theta_v - \cos\theta_Y)$, F_p is the static friction force and its maximum value is approximate to $\eta\gamma_{ci}$,[24] where $\eta = \varepsilon_0\varepsilon_r/2d\gamma_{ci}V^2$. Then the first threshold potential V_{Th1} is derived as

$$V_{Th1} = \sqrt{\frac{2d\gamma_{ci}(\cos\theta_V - \cos\theta_Y)}{\varepsilon_0\varepsilon_r}}. \tag{21}$$

When voltage increases to V_{Th2}, the electrowetting force value $F_{el} = \varepsilon_0\varepsilon_r/2dV^2$ starts to exceed the capillary force $F_{cap} = \gamma_{ci}(\cos\theta_v - \cos\theta_Y)$, the surface tension γ of the conducting fluid and static friction forces. Before the contact line moves and contact angle decreases, the ions start to break the fluid bondage because of the lower interfacial energy, escape from main drop and then lead to electrowetting saturation. By eliminating the static friction force F_P, we can have

$$\frac{\varepsilon_0\varepsilon_r}{2d}(V_{Th2} - V_{Th1})^2 = \gamma_{ci}(\cos\theta_v - \cos\theta_Y) + \gamma. \tag{22}$$

Rearranging Eq. (22) leads to

$$V_{Th2} = V_{Th1} + \sqrt{\frac{2d\gamma_{ci}}{\varepsilon_0\varepsilon_r}(\cos\theta_v - \cos\theta_Y) + \frac{2d\gamma}{\varepsilon_0\varepsilon_r}}. \tag{23}$$

3. Results and discussion

A series of experiments is implemented to verify the validity of the proposed theoretical model. The photos of electrowetting are shown in Fig. 2, and also the diagrams of the basic electrowetting testing setup are shown in the inset of Fig. 2. The complete substrates coated with parylene C ($d = 3.6$ μm, $\varepsilon_r = 3.15$) and CYTOP (~ 50 nm thickness) are placed in a clear acrylic box and immersed in an insulating fluid. The conductive fluids are deposited with a pipette (drop 0.5 μl) and electrically biased through the insertion of a tungsten probe tip (10 μm in diameter) connected to a Trek power amplifier (model 603) coupled to a Tektronix AFG 3022B function generator. The contact angle change is monitored and measured with drop shape analysis systems (software version 2.0), which are repeated 3 times at fresh sample locations.

The insulating fluid and the conductive fluid employed in Fig. 2 are isopar oil with surface tension $\gamma_{isopar} = 27$ mN/m

and propylene glycol with surface tension $\gamma = 35$ mN/m), respectively, and the interfacial tension between propylene glycol and isopar oil is $\gamma_{ci} = 9.957$ mN/m. Figure 2 shows that the correlated initial contact angle θ_Y is about 156° and the final saturating contact angle approaches to ~15°. When $V \geq 150$ V, the saturating contact angle occurs, which is characterized by many micro-jet satellite droplets accumulating around the main droplet instead of dielectric breakdown.

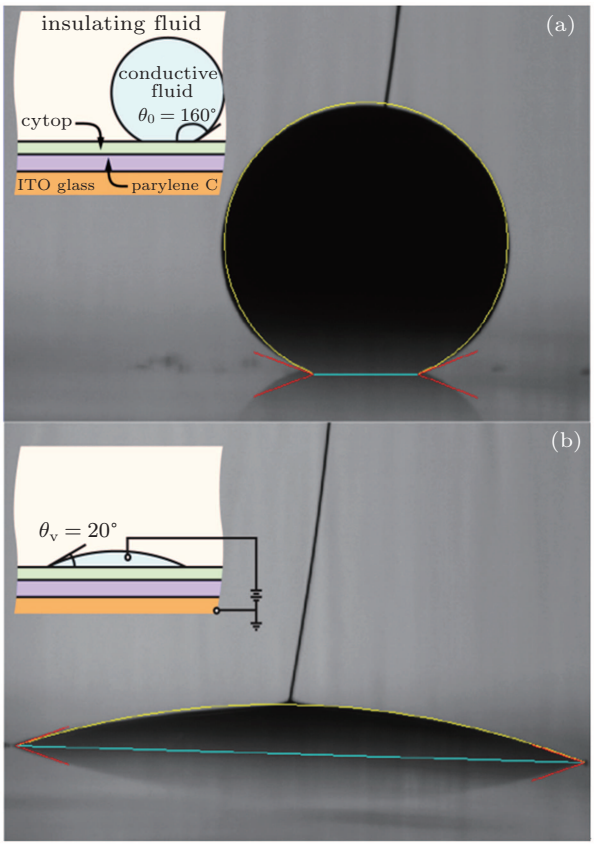


Fig. 2. (color online) Diagrams and photos of electrowetting at (a) 0 V and (b) 180 V.

Figure 3 shows the variations of measured contact angle with voltage (■: experimental data) and their comparisons with the results predicted by the Young–Lippmann equation (●: Young–Lippmann equation) and our theoretical model Eq. (19) (▲: theoretical model). Since the Young–Lippmann equation ignores the energy dissipation during the droplet spreading, it starts to deviate from the experimental data curve at the point voltage $V = 37.5$ V and decreases to zero sharply. As a matter of fact, the contact angle observed in the experiment continues to decrease slowly when $V \geq 37.5$ V and eventually keeps constant when voltage $V \geq 150$ V. Our theoretical curve predicts the evolution of the transient contact angle in electrowetting, which shows good consistence with the relevant experimental results. They show that the contact angle decreases sharply in the beginning, and then declines slowly during the second stage, and finally it evolves into the saturation state. In Fig. 3, the point potentials $V_1 = 37.5$ V and $V_2 = 150$ V correspond to the first and second threshold potential V_{Th1} and V_{Th2} respectively in our theory, which are calculated via Eqs. (21) and (23). Substituting $\gamma_{ci} = 9.957$ mN/m, d = 3.6 μm, $F_{el} = 2\eta\gamma_{ci}$, $\varepsilon_0 = 8.85\times10^{-12}$, $\varepsilon_r = 3.15$, $\theta_Y = 156°$, $V = 37.5$ V, and $\theta_v = 117°$ into Eq. (21), we obtain the first theoretical threshold potential $V_{Th1} = 34.5$ V. Employing Eq. (23), the second theoretical threshold potential $V_{Th2} = 117.9 + V_{Th1} = 152.4$ V is calculated at $V = 150$ V and $\theta_v = 15°$ by the following parameters: $\gamma_{ci} = 9.957$ mN/m, $d = 3.6$ μm, $\varepsilon_0 = 8.85\times10^{-12}$, $\varepsilon_r = 3.15$, $\gamma = 35$ mN/m, $V_{Th1} = 34.5$ V, and $\theta_Y = 156°$. Obviously, our theoretical threshold potentials $V_{Th1} = 34.5$ V and $V_{Th2} = 152.4$ V are in good agreement with the experimental values $V_1 = 37.5$ V and $V_2 = 150$ V, respectively.

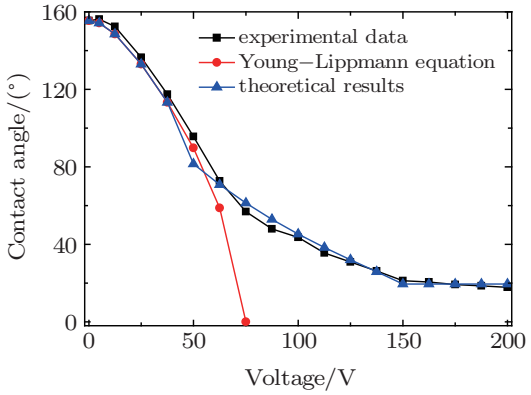


Fig. 3. (color online) Comparison of plot of contact angle versus applied voltage among experimental data (■), results from Young–Lippmann equation (●), and theoretical data (▲).

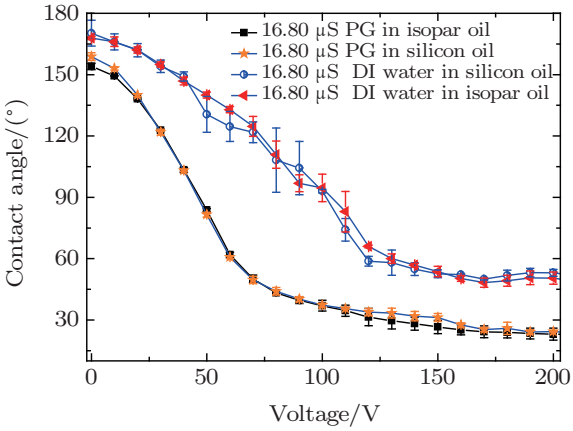


Fig. 4. (color online) Plots of contact angle versus applied voltage for different combinations of conductive and insulating fluid.

To elucidate the influences of interfacial and surface tension on electrowetting behavior more clearly, different combinations of conductive and insulating fluids with the same conductivity are employed for the test, and the results are shown in Fig. 4. The insulating fluids include a blend of Dow Corning OS silicone oils (80 wt% OS-20, 10 wt% OS-10, and 10 wt% OS-30, $\gamma_{silicone} = 21$ mN/m) and a hydrocarbon blend (Isopar M, C11–C16 isoalkanes with <2% aromatics,

γ_{isopar} = 27 mN/m), while the conductive fluids include propylene glycol (TBA-Ac, 5% black Pigment, γ_{PG} = 35 mN/m) and DI water (γ_{DI} = 73 mN/m). From Fig. 4, we can find that the conductive fluid dominates the saturating contact angle size and the onset of electrowetting saturation while the influence of insulating fluid on electrowetting saturation is negligible. It is also remarkable that good system stability performance, as shown by the small error bar, is achieved by employing propylene glycol as the conductive fluid.

Figure 5 shows the discrepancies in the saturating contact angle among different surface tensions of conductive fluid in isopar oil, where conductive fluid and isopar oil have the same conductivity. It again confirms that the magnitude of the saturating contact angle increases with the surface tension of conductive fluid, and the minimum saturating contact angle is about 25° for pure propylene glycol (PG) while that of DI water is around 50°, which is attributed to the difference of surface tension between the different conductive fluids. According to surface free energy theory, to reduce the contact angle, electrostatic force is required to overcome ion binding energy and then drive a certain number of internal ions (or charges) to the surface of the droplet.[25] Hence, it implies that the smaller the surface tension of the conductive fluid, the smaller the electrostatic energy consumed by one ion (or charge) migrating from inside to the interfacial surface. Since the surface tension of propylene glycol ($\gamma \sim 35$ mN/m) is smaller than that of DI water ($\gamma \sim 73$ mN/m), much more internal ions (or charges) in PG are driven to the surface under the same applied voltage, and consequently a lower saturating contact angle is achieved.

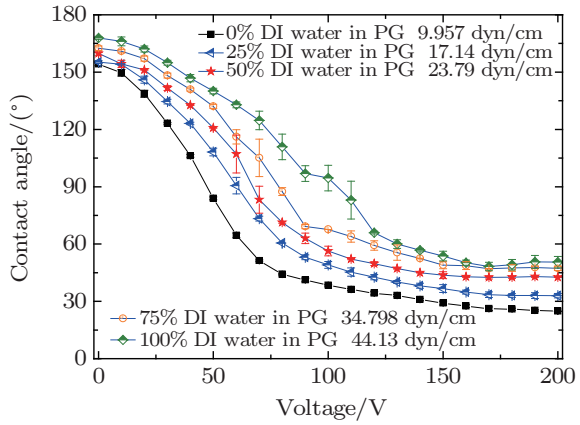


Fig. 5. (color online) Plots of contact angle versus voltage for different volume percentages of DI water in PG, where DI water and PG have the same conductivity 16.8 μS.

Figure 5 also shows that the smaller the interfacial tension of the 3-phase system, the earlier the onset of the saturating contact angle is. It can be found in Figs. 4 and 5 that compared with pure DI water, the conductive fluid comprised pure PG reaches the contact angle saturation earlier, i.e., $V_{th2,PG} < V_{th2,water}$, which is in agreement with the results of Chevalliot *et al.*[26] Since the interfacial tension of PG and insulating fluid ($\gamma_{ci,PG}$ = 9.957 mN/m) is smaller than that of DI water and insulating fluid ($\gamma_{ci,water}$ = 43 mN/m), the corresponding interface binding energy, the energy that one escaping ion in PG needs to overcome, is smaller. When the applied voltage is increased to a certain value, the electrostatic energy is powerful enough to drive the ions in PG into migrating to the interface and escaping from the main droplet while inner ions in DI water are still bound tightly. Therefore, it seems to be reasonable to conclude that saturation is triggered when ions are pulled from the main droplet and it is dominated by the interfacial tension, which is consistent with Liu *et al.*'s results.[25]

4. Conclusions

This work focuses on the exploration of the physical origin of electrowetting saturation, approaches to lowering the saturating contact angle, and the construction of a theoretical model for calculating the threshold potential and describing electrowetting behavior. Proper combination of the 3-phase system employed succeeds in dropping the saturating contact angle below 25° and achieving a good system stability performance. The theoretical model established to predict the transient contact angle change with higher potential shows good agreement with the relevant experiments. As for the electrowetting saturation, it is triggered once ions (or charges) escape through the interface of the droplet. A 3-phase system with higher interfacial tension and lower surface tension of conductive liquid facilitates to generate the lower contact angle and delay the formation of electrowetting saturation. The relevant results will enrich the research of electrowetting, promote the application in the area of micro-optics and optoelectronic information technology, and thus expand its application scope.

Acknowledgment

We thank Dr. Di Li (Shandong University of Technology) for many useful discussions and comments, and also thank the Novel Devices Laboratory, University of Cincinnati, USA for the access to major fabrication and EW measurement and their various contributions to the EW work.

References

[1] Sista R, Hua Z, Thwar P, Sudarsan A, Srinivasan V, Eckhardt A, Pollack M and Pamula V 2008 *Lab on a Chip* **8** 2091
[2] Lazar I M and Kabulski J L 2013 *Lab on a Chip* **13** 2055
[3] Mugele F and Baret J C 2005 *J. Phys.: Condens. Matter* **17** R705
[4] Peng R L, Chen J B and Zhuang S L 2008 *J. Opt. Soc. Am. A* **25** 2644
[5] Berge B and Peseux J 2000 *Eur. Phys. J. E* **3** 159
[6] Hayes R A and Feenstra B J 2003 *Nature* **425** 383

[7] Hagedon M, Yang S, Russell A and Heikenfeld J 2012 *Nat. Commun.* **3** 1173
[8] Yuan Q Z and Zhao Y P 2010 *Phys. Rev. Lett.* **104** 246101
[9] Mugele F 2009 *Soft Matter* **5** 3377
[10] Papathanasiou A G, Papaioannou A T and Boudouvis A G 2008 *J. Appl. Phys.* **103** 034901
[11] Drygiannakis A I, Papathanasiou A G and Boudouvis A G 2008 *Langmuir* **25** 147
[12] Quinn A, Sedev R and Ralston J 2005 *J. Phys. Chem. B* **109** 6268
[13] Kedzierski J T, Batra R, Berry S, Guha I and Abedian B 2013 *J. Appl. Phys.* **114** 024901
[14] Vallet M, Vallade M and Berge B 1999 *Eur. Phys. J. B* **11** 583
[15] Yuan Q Z and Zhao Y P 2015 *Nanoscale* **7** 2561
[16] Gupta R, Sheth D, Boone T, Sevilla A and Frechette J 2011 *Langmuir* **27** 14923
[17] Buehrle J, Herminghaus S and Mugele F 2003 *Phys. Rev. Lett.* **91** 086101
[18] Mugele F and Buehrle J 2007 *J. Phys.: Condens. Matter* **19** 375112
[19] Verheijen H J J and Prins M W J 1999 *Langmuir* **15** 6616
[20] Oprins H, Vandevelde B and Baelmans M 2012 *Micromachines* **3** 150
[21] Ren H, Fair R B, Pollack M G and Shaughnessy E J 2002 *Sensors and Actuators B: Chemical* **87** 201
[22] Brochard F 1989 *Langmuir* **5** 432
[23] Nelson W C and Kim C J 2012 *J. Adh. Sci. Technol.* **26** 1747
[24] Li F and Mugele F 2008 *Appl. Phys. Lett.* **92** 244108
[25] Liu J, Wang M, Chen S and Robbins M O 2012 *Phys. Rev. Lett.* **108** 216101
[26] Chevalliot S, Kuiper S and Heikenfeld J 2012 *J. Adh. Sci. Technol.* **26** 1909